LFNN #1283618, VOL 0, ISS 0

Fullerenic-topological tools for honeycomb nanomechanics. Toward a fullerenic approach to brain functions

Arturo Tozzi, James F. Peters, and Ottorino Ori

QUERY SHEET

This page lists questions we have about your paper. The numbers displayed at left can be found in the text of the paper for reference. In addition, please review your paper as a whole for correctness.

Q1. Au: Please provide publisher name and location for Ref. 5.
Q2. Au: Please provide publisher name and location for Ref. 6.

TABLE OF CONTENTS LISTING

The table of contents for the journal will list your paper exactly as it appears below:

Fullerenic-topological tools for honeycomb nanomechanics. Toward a fullerenic approach to brain functions
Arturo Tozzi, James F. Peters, and Ottorino Ori

FULLERENES, NANOTUBES AND CARBON NANOSTRUCTURES
2017, VOL. 0, NO. 0, 1–7
http://dx.doi.org/10.1080/1536383X.2017.1283618

Taylor & Francis
Taylor & Francis Group

Fullerenic-topological tools for honeycomb nanomechanics. Toward a fullerenic approach to brain functions

Arturo Tozzi[a], James F. Peters[b], and Ottorino Ori[c]

[a]Center for Nonlinear Science, University of North Texas, 1155 Union Circle, #311427, Denton, TX, USA; [b]Department of Electrical and Computer Engineering, University of Manitoba, 75A Chancellor's Circle, Winnipeg, Canada; [c]Actinium Chemical Research, Via Casilina 1626/A, Rome, Italy

ABSTRACT

Fullerenic structures equipped with Stone-Wales transformations have been successfully utilized in the study of macromolecular assemblies. Here we show that this approach could be useful in the assessment of issues from a far-flung research area, i.e., neuroscience. Indeed, the basic morphological and functional unit of the brain, called the human microcolumn, is a tubular structure that can be flattened in the guise of a fullerene-like two-dimensional lattice. We describe this procedure in order to build a fullerene-like microcolumn, in which neuronal firing and electric signal propagation are assessed in terms of topological neural network modifications, instead of the canonical logic circuits. Every node stands for a neuron, where neural computations take place. This means that nervous activity, other than logic circuits, could instead depend on topological transformations and symmetry constraints dictated by Stone-Wales transformations occurring in the upper cortical layers. A two-dimensional fullerene-like lattice not only simulates the real microcolumn's microcircuitry, but also makes it possible us to build artificial networks equipped with robustness, plasticity and fastness. In this note, electric signal propagation is investigated in terms of pure topological modifications of the neural honeycomb network.

KEYWORDS

Brain topology; Fullerene-like lattice; Stone-Wales transformations; Topological efficiency, Simplicial complex

1. Introduction

Although fullerenes' primary application focuses on the assessment of carbon-networks in nanostructures, they also provide a mathematical framework that can be used in order to rank topological invariants in the portrayal of microcolumns, i.e., the stereotyped, column-like architecture representing the basic embryological/anatomical arrangement of the brain (1,2). Because architectonic relations among minicolumnar pyramidal cells are conserved under spatiotemporal changes (3), it is feasible to assess the tubular structure of the brain in terms of a 3D cylinder with the typical regular polygonal tiling of the fullerene. If we flatten the microcolumnar cylindrical structure to obtain of two-dimensional sheets, we achieve a lattice where generalized Stone-Wales transformations (or SW rotations) might occur (4,5). Therefore, it is possible to achieve a fullerene-like brain microstructure in which activity is dictated by transformations involving fullerene-like polygons. In a fullerene-like microcolumn, neuronal firing is assessed in terms of untangled topological neural network transformations. This structure can be compared to a barcode, or a biological matrix, in which every sequence of neuronal activation stands for a mental activity. We may also think of the bronze cup-shaped bells of a carillon, in which every sequence of diverse punchers gives rise to different melodies. In sum, we achieve a fullerene-like brain whose activity is dictated by topological transformations involving hexagons, pentagons, and other polygons. Such an approach not only allows us to build a model that faithfully simulates the biological brain activity, but also to assess neural computations in terms of topological relationships and transformations among spiking neurons, instead of series or parallel logic circuits. We also discuss the advantages of such an approach in terms of network fastness, robustness and plasticity.

Neuronal firing and electric signal propagation can be investigated in terms of SW topological modifications of the neural network. This assumption leads to a characterization of neurons as graph vertices and connections among neurons as bonds. Because such transformations are fully reversible, they provide a biological topological mechanism for neural signal annihilation or suppression. Concerning the mathematical apparatus related to symmetries and transformations on nanostructures, see the recent research article (6). Microcolumnar circuitry can be described in terms of fullerene-like 2D lattices with correlations between cell topology and computational models to describe circuitry functionalities (7). We are in fact allowed to build a biologically-plausible, fullerene-like lattice describing a microcolumn, equipped with hexagonal or pentagonal tiling. There are clues from the neuroscientific literature that suggests the feasibility of our hypothesis. Minicolumns are characterized by modular connectivity with invariant properties that resemble fullerene structures. Indeed, minicolumns display a translational symmetry across their central axis and rotational symmetry, i.e., displacement in different planes of each section. Furthermore, microcolumns are equipped with

CONTACT Ottorino Ori ottorino.ori@alice.it Actinium Chemical Research, Via Casilina 1626/A, 00133 Rome, Italy.
Color versions of one or more of the figures in the article can be found online at www.tandfonline.com/lfnn.

both transitive symmetry involving geometric scaling of morphometric relations in different cortical areas, and temporal symmetry involving morphometric relations during cortical maturation (29). Because architectonic relations among minicolumnar elements (pyramidal cells) are conserved under spatial and temporal variations (30), it is possible to assess the tubular structure of a microcolumn in terms of a 3D cylinder with the typical regular structure of the fullerene, e.g., a mesh of variously fused exagons and pentagons. Furthermore, it has been demonstrated that the microcortical assembly of pyramidal neurons exhibits the required fullerene-like stereotyped architecture. Indeed, neurons arranged in a parallel microcolumns' hexagonal lattice have been already described in literature (31). The hexagonal lattice is a reasonable assumption for microcolumns arrangement, based on studies of dendritic bundles and myelinated axons packing. Hexagonal spacing has been detected among bundles in the visual cortex' area 17 of rats (33), monkeys (34), and human medial prefrontal cortex (32)

In this graphical representation of the brain, nodes stand for microcortical pyramidal neurons linked by edges, e.g., neural dendritic connections. In cortical microcolumns, instead of SW flips on a fullerene surface, we need to evaluate the changes in firing activation of the neurons embedded in the nodes. In this case, SW permutations stand for a set of simple pyramidal neurons which fire simultaneously (Fig. 1). Therefore, it is possible to achieve a 2D fullerene-like lattice reproducing microcolumn's microcircuitry. We assume that the simultaneous firing of different neurons and specific activation sequences might give rise to *different topological isomeric conformations*, each one corresponding to a mental activity (perception, emotion, mind-wandering, calculation, and so on). The main difference from classical neural networks is that the brain functional activity is not based on logic nodes as it occurs in conventional networks, but on topological transformations, e.g., functional changes in the connectivity of firing neurons on a barcodelike structure. This model explains *countless* mental operations starting just from a relatively simple, stereotyped, highly preserved biological structure, such as the microcolumn. The extremely large number of SW rotations that may take place on the neural lattice permit an almost limitless set of moves, merely dictated by applying SW rotations on its bonds. In the same way as the tuning of the nanoparticle/substrate interaction provides unique ways of controlling the nanotube synthesis (8), fullerene-like, microcolumnar neural networks provide the fine-grain functional barcode's modularity required by different brain functions. This means that modifications in reciprocal connectivity among adjacent microcolumns allow a larger repertoire of barcode configurations and, therefore, of mental operations. In mental terms, a fullerene-like microcolumnar structure is associated with minimal wiring costs and fast synchronization/information transfer (9).

Topological and graph theoretical properties of fullerenes can be applied to the assessment of neural networks, in order to achieve a double task: improving our understanding of biological brain function in situ, and building more powerful artificial machines able to simulate cortical activities. This theoretical framework, cast in a biologically informed fashion (10–12), has the potential to be operationalized and assessed empirically. Indeed, the presence of a microcolumnar barcode

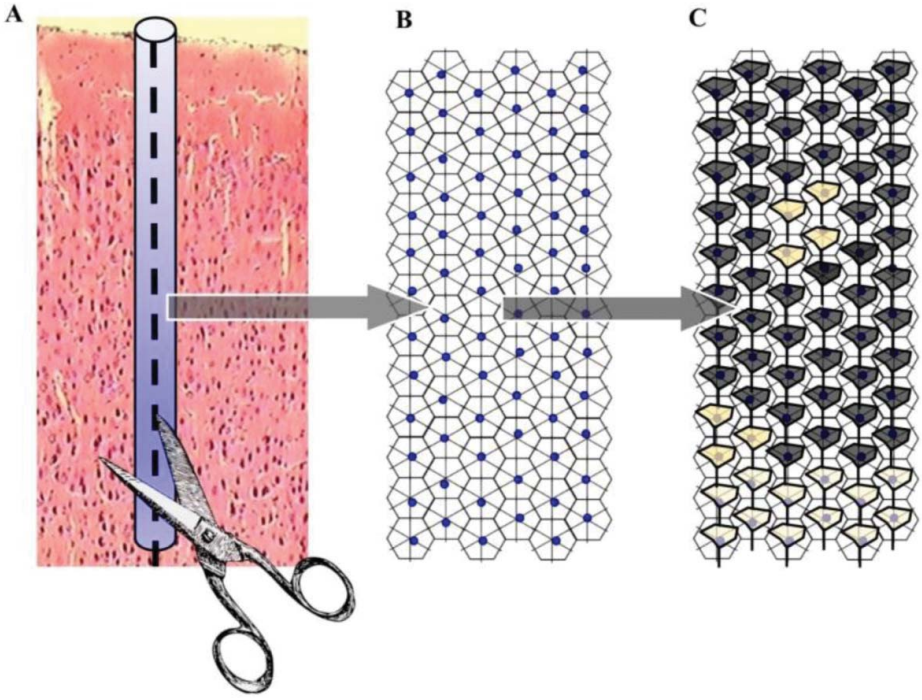

Figure 1. A fullerene-like cortical microcolumn. (A) The anatomical/functional basic structure of the brain, i.e., the tiny cortical microcolumn, is shaped in guise of a three-dimensional tubular armchair. If we cut the column through an edge, we achieve a flattened two-dimensional fullerene-like grid with exagonal tiling (B). In the hypothetical case of (B), provided just as an example, the molecular graph stands for a 2D zig-zag lattice, e.g., a flat, open visualization, made of 72 nodes with 6-bonds each. Panel (C) displays a set of possible topological transformations that might take place on this flattened microcolumn. Every node is filled with a pyramidal neuron which can be activated (yellow shapes) or deactivated (black shapes). Every set of activated/deactivated neurons gives rise to a different microcolumnar code, each one standing for a single mental activity among the countless possible.

predicted by a fullerene-like brain will be easily testable, once more powerful high density neurotechniques will be available, capable of capturing the simultaneous activity of large populations of microcolumnar pyramidal neurons. Graph theory tools have been proven to work quite effectively in simulating neuronal networks and relevant studies have been recently devoted to overcome what is considered to be a "critical simplifying assumption", i.e., that the basic unit in brain structure consists in just two nodes (a *dyad* of neurons or brain regions) connected by a graph edge. Generalized forms of graphs (*simplicial complexes*) based on algebraic topology recently appeared in literature (13) to model neural data and neural functions without the *dyadic limit*, aiming in such a [illegible] to "eclipse graph theory" in the n[illegible] future of neural s[illegible]ces. These sophisticated (somehow [illegible]itrarily applicable) mathematical methods may be, in the opinion of the present authors, better applied by computing opportune n[illegible]cal *topological invariants* (or *topological potentials*) that [illegible] the clear merits of carrying-on the influence of the structure of the whole neural network, keeping at the same time, uniquely defined computational rules. T[illegible] present topological picture enlarges the horizon of recently reported methods that have been applied to simulate mechanical properties of zigzag honeycombs (see, e.g., (14)). In sum, original relationships between *neural signals* [illegible] *topological defects* are proposed in the follo[illegible]g sections [illegible]ether with a specific theoretical framework th[illegible]able to describe the nanomechanics of 3-connected neural networks regardless of their structural regularities.

2. Topological method

In this section, we describe the procedure in order to build a fullerene-like microcolumn, in which neuronal firing and electric signal propagation are assessed in terms of pure topological neural network modifications, instead of the canonical ON/OFF logic circuits. At first, we illustrate how to shape a fullerene-like lattice through graph theoretical methods. Then, we evaluate the (*fully reversible*) topological moves taking place on such a lattice. Finally, we assess the neural biological counterparts of fullerenic structures, assessing microcolumns and neural spikings in terms of movements on [illegible]per 2D graphs. Furthermore, we provide, in the last section, a couple of simulations in order to test the feasibility of our fullerene-like microcolumnar framework.

Fullerene networks come into play. Fullerenes are 3-connected cubic planar graphs consisting of pentagons and hexagons; see the excellent recent update (15). Geometrically, a C_n fullerene is a closed trivalent polyhedral network in which n atoms are arranged in 12 pentagonal and $\left(\frac{1}{2}n-10\right)$ hexagonal rings (16–18). A regular 2D fullerene results therefore in a 3-regular (cubic) planar graph G_n generally describable as a mesh of exactly 12 variously fused pentagons, surrounded by distorted graphenic fragments. Signal propagation can be investigated via graph theoretical methods in this kind of cubic meshes. The basic assumption is that the evolution of microcircuits is ruled by the minimization of specific *topological invariants* (or *topological potential*) Ξ. Among the countless possible choices (19), we focus here on *distance-based* topological invariants capable of describing *long-range effects* involving *all pairs* of graph nodes.

The honeycomb microcircuit is described as a graph G_n with n nodes in which the d_{ij} integers stands for the number of graph edges connecting the two nodes i and j along the shortest path. In case of the distance $d_{ij}=k$, node j belongs to the k-th coordination shell of node i, and vice versa. By definition, $d_{ij}=d_{ji}$ and $d_{ii}=0$ for all nodes i,j. If we term $M=\max\{d_{ji}\}$ the length of the longest chemical distance in the graph—the integer M stands then for the graph *diameter*— and b_{ik} the number of k-neighbors of i, the effects of the long-range connectivity on a single node is summarized by the topological invariant w_i in (1).

$$w_i = {}^1\!/_2 \sum\nolimits_k k b_{ik} \quad k = 1, 2, \ldots, M-1, M, \qquad (1)$$

where $n=\Sigma_k b_{ik}+1$ and $b_{i1}=6$ for any 6-fold node i. The symbols $\underline{w}$ and $\overline{w}$ indicate the smallest and the largest w_i values. Nodes with $w_i=\underline{w}$ (or $w_i=\overline{w}$) are the *minimal nodes* (or, conversely, the *maximal nodes*) in G_n. Integers $\{b_{ik}\}$ identify the Wiener-weights (WW) of node i. The Wiener index W, i.e., the first topological index applied in chemistry more than 60 years ago (19), derives from the half-summation of all d_{ij} entries given in (2).

$$W(n) = {}^1\!/_2 \sum\nolimits_{ij} d_{ij} = \sum\nolimits_i w_i \quad i,j = 1, 2, \ldots, n-1, n. \qquad (2)$$

The first topological modeling rule is the following: higher reactivity is assigned to a node with maximal w_i. Invariant W, providing the topological measure of the overall compactness of the system, is a good candidate for the topological potential $\Xi^W = W(G_n)$. This approach is grounded on relevant heuristic evidences, such as the fact that, among the 1812 nonisomorphic C_{60} fullerene isomers, just the physically stable isomer with icosahedral symmetry C_{60}-I_h and isolated pentagons corresponds to the cage with the minimum value $W=8340$ and it works well in marking stable isomers of C_{28}, C_{66} fullerenes (20, 21). The descriptor in (3)

$$\rho = W/n\underline{w} \qquad (3)$$

measures instead the overall ability of the graph to evolve as a compact topological structure around its minimal nodes, which represent the most efficient nodes in G_n. For this reason ρ is called a *topological efficiency* index (20) and has been successfully tested to rank the *topological sphericity* of C_{50} fullerene graphs (22). From formula (3), an important inequality is derived, namely, the result in (4)

$$\rho \geq 1 \qquad (4)$$

Many important chemical structures have $\rho=1$. Infinite cubic lattices or infinite graphene layers, together with icosahedral C_{60} molecules, are examples of perfectly spherical (topologically speaking) structures. And we formulate the second topological modeling rule: *the higher stability is assigned to structures with maximal sphericity*, e.g., minimal ρ. The two above mentioned modeling rules hold when similar topological

structures are compared. Lattice descriptor ρ represents in this approach the second form of topological potential $\Xi^{\rho} = \rho\,(G_n)$; both potentials Ξ^{W} and Ξ^{ρ} measure the collective effects exerted by G_n nodes on the nanomechanics of honeycomb mesh, including signal propagations effects.

3. Results and discussions

Preliminary simulations show how, starting from a fullerenic structure, it is possible to reversibly generate many alternative isomers (usually with a lower structural symmetry) by twisting two hexagons around a central bond (Fig. 2). The mechanism of signal generation is based on the preliminary activation of a pair of neurons both in the normal 6-fold status, followed by the creation of the *signal*, e.g., a *topological defect* of the pristine hexagonal mesh, that is represented by the 5|7 double pair (Fig. 2: step 0 and step 1, respectively). The 5|7 double pair (sometimes termed 5/7/7/5) is called the *SW defect* or *dislocation dipole*. Signal generation is achieved through the $SW_{6|6}$ rotation. The latter modifies the local connections of four neurons by rotating the bond between the two activated elements. After that change of local connections, nodes with 5- and 7-bonds appear in the network, making the topological structure of the system "naturally" ready for signal propagation that is easily obtained by applying a $SW_{6|7}$ rotation to the connection between the newly created 7-fold neuron and the activated one (Fig. 2, step 2), preserving the original 6-connectivity. As a result of the $SW_{6|7}$ action, the distance between the two 5|7 defects is increased by the insertion of one pair of hexagons, so that the signal has travelled for one step $\eta = 1$ in the honeycomb mesh. The two neurons that are brought back to the initial 6-fold condition (Fig. e 2, step 3) stand for the inactive status and their role will be briefly commented at the end of this section. Successive applications of $SW_{6|7}$ operators will split more and more of the two 5|7 pairs, allowing the signal to travel in the neural network with the typical wave mechanism of the SWw topological defect (23). Figure 2, step 4 shows the dislocation dipole with length $\eta = 2$; subsequent $SW_{6|7}$ rotations will further expand the dislocation dipole, allowing the topological signal to cover arbitrary distances η. According to the proposed approach, the large family of SW rearrangements introduced above, such as $SW_{6|6}$, $SW_{6|7}$ and so on, provide us with the basic tools in order to build a topological model able to describe the signal propagations in the neuron mesh. In summary, the topological mechanism describing the propagations of neural signals is based on the following graphical steps:

- The signal is considered to be a topological defect of the neural network. The "topological" benefits are straightforward: the signal does not change the number of neurons, being easily annihilated by the reverse topological transformation able to restore the original status of the neural network. In principle, this fact also allows long duration of the network itself.
- The specific type of topological alteration proposed here as proper candidate for representing neural signal is the

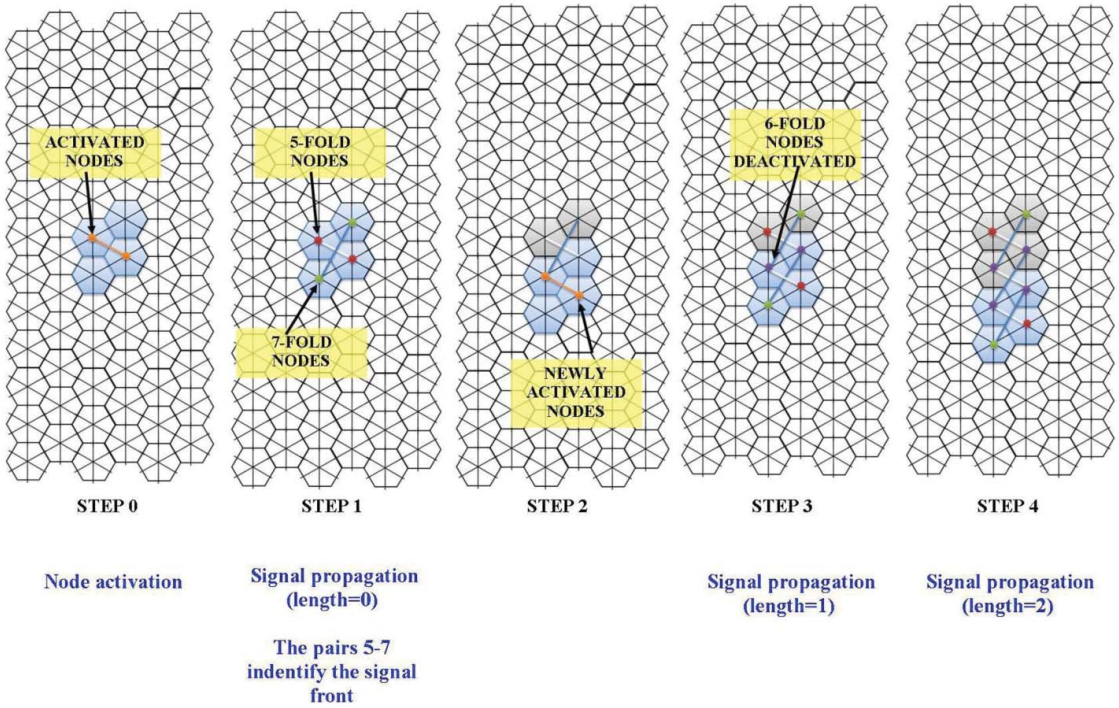

Figure 2. Simulation of a few possible transformations taking place on a flat exagonal lattice equipped with 72 nodes, 6-bonds each. The lattice stands for the cortical microcolumn containing 72 pyramidal neurons described in Figure 3C. Starting from the totally inactive state of 6-fold nodes on 6×12 lattice, some nodes gets activated (STEP 0). We may select whatever pair in the mesh. To make an example, after a visual input from the external environment, a few microcolumnar pyramidal neurons start to fire. STEP1 displays two 5|7 pairs, activated by just rotating the orange bond of STEP 0. Signal propagation gives rise to a sequential activation of novel front nodes (STEP 2), so that the activation wave propagates steps further (STEPS 3 and 4). Note that the purple balls, which identify hexagonal nodes deactivated after the passage of the wave, are ready for a possible reversible annihilation of the topological signal.

SW defect formed by two 5|7 pairs, whose creation involves 4 connected neurons under the action of the $SW_{6|6}$ operator.

- Multiple applications, for η-times, of the $SW_{6|7}$ operator produce the SWw defect with the expansion of the SW dislocation dipole and the linear propagation of the signal, in order to cover the distance η. The size η of the SW dislocation dipole (e.g., the signal) also corresponds to the number of pairs of inactive neurons included between the two 5|7 pairs. This topological modification of the network is also indicated as $5/7\{6/6\}_\eta 7/5$. SW defect has then $\eta = 0$.
- If needed, the η pairs of inactive neurons allow the complete topological annihilation of the SW dislocation dipole, by just applying η-times the reverse $rSW_{6|7}$ flip. The $rSW_{6|6}$ rotation will then restore the pristine hexagonal lattice.

The proposed correspondence between the neural signal and the linear SWw defect is just the simplest choice in the large family of topological modifications of the neuron lattice that may be built via SW rotations. The possible combinations of permutations (and therefore of simultaneously activated neurons in a fullerene-like microcolumn) are countless: in a lattice of 80 nodes and 2 activities (ON/OFF), we achieve the noteworthy number of 2^{80} possible permutations. Many operations, not shown in Figures, can be performed: edge sharing, interchanging the positions of two hexagons, rotation of a single edge, and so on. Because the switches are fully reversible, the edges can be rearranged in countless ways.

We do not know, due to our current lack of knowledge, whether the microcortical assembly of pyramidal neurons truly exhibits the required fullerene-like stereotyped conformation. The Borsuk-Ulam theorem (BUT) from algebraic topology, ideally suited for many applications (24), gives us a clue to solve this problem. The original formulation of BUT describes antipodal points on an n-sphere with matching descriptions on spatial manifolds in every dimension, provided the n-sphere containing the antipodes is a convex structure with positive curvature (i.e., a ball). However, BUT can be generalized to symmetries occurring either on flat manifolds, or on Riemannian hyperbolic manifolds of constant sectional curvature -1 and concave shape (i.e., a saddle) (12, 25). In other words, whether the system components are equipped with concave, convex or flat conformation, it does not matter: we can always find points with matching descriptions predicted by BUT (26).

The modifications of the *long-range structure of honeycomb network topology* depicted in Fig. 2, may be modeled by computing both topological potentials Wiener index $W(n)$ and topological efficiency index $\rho(n)$ introduced in the previous section (eqs. 3 and 4). The topological propagation of the signal has been simulated on the dual neural lattice G_n consisting of $n = 72$ nodes, all 6-connected, with $B = 216$ total edges due to periodic boundary conditions. That pristine graph G_n^* is then characterized by the starting values $W_n^* = 9864$; $\rho_n^* = 1$ of the two lattice descriptors (Fig. 3). Computation shows the 0.73% gain of the Wiener index when it passes to $W_n^0 = 9792$ after the creation of the SW defect with $\eta = 0$. The subsequent $SW_{6/7}$ initiates, by shifting one of the 5|7 pair in the lattice, the propagation of the signal further decreasing the topological potential $W_n^1 = 9771$ and $W_n^2 = 9728$ for $\eta = 1$ and $\eta = 2$, receptively. This behavior confirms that, at each propagation step, the expanding SWw defect increases the overall compactness of the neural network G_n^η, augmenting in such a way the *topological stability of the honeycomb system itself*. The global drop of the *topological potential* Ξ^W, shown in Fig. 3(a), demonstrates a linear trend favoring signal propagation. After the creation of the SW defect $\eta = 0$, the invariants w_i of the 72 neurons leave the uniform value $\underline{w} = 137$, assuming that different values depend on the respective topological stability. The two heptagons become the two stables nodes with $_{w\_} = 130$; vice versa, the two pentagons are the less stable nodes of the neural mesh with maximal value $\overline{w_n^0} = 138$. As shown in Fig. 3b, the topological potential Ξ^ρ provides more details about topological rearrangements of the honeycomb mesh during signal propagation. The increased value of topological efficiency $\rho_n^0 = 1.0462$ stands for the barrier in the topological potential that competes against the signal creation. After this point, the topological potential Ξ^ρ shows a regular decrease, favoring in such way the smooth expansion of the SW dislocation dipole, e.g., the topological defect carrying the signal in the graph.

In this note, we showed how SW transformations might have a counterpart in the biological activity of brain microcircuitry. The results provided by the present study sustain the proposed original coincidence between *neural signal & topological defects*. We make available a novel approach that allows us to evaluate brain activity in terms of topological and graph theoretical properties of fullerenes. In touch with neural networks derived from the principle of minimum frustration for protein folding (27), the fullerene-like approach points towards a perception/decision apparatus constrained towards very low energetic levels, but just in long timescales, in order that predictions signals are conveyed by the sole long-standing past experiences. This is a very fertile field of research: current efforts focus on the unsolved mathematical problems concerning fullerenes, e.g., how to generate all possible non-isomorphic graphs for a fixed vertex count, or to calculate the number of distinct Hamiltonian cycles. Researchers are developing 2D graphs and 3D structures for many different fullerenes, ranging from $N = 20$ to 20,000 vertices, in order to evaluate various different graph-theoretical algorithms (28) and theorems and algorithms which allow a fast computation of topological indices for complex graphs, starting from their structural building elements (6). Future investigations will be carried out to correlate the sequences of SW topological transformations to the isomeric generation and propagation of 5|7 pairs or similar topological extended defects in the neural mesh.

Our framework also provides a link with human neurologic and psychiatric diseases. Experimental data and molecular dynamic simulations suggest that defects during the nucleation and growth of graphene alter the physical/chemical properties of carbon nanostructures (35), strongly deteriorating their functional state. An increase in energetic constraints, as it occurs, for example, during ageing or central nervous system's diseases, makes it easy to generate defects in the microcolumnar fullerene-like lattice, with subsequent decrease in system's free-energy and functional integrity. Our theoretical framework, cast in a biologically informed fashion, has the potential to be operationalized and assessed empirically. Indeed, the presence of a

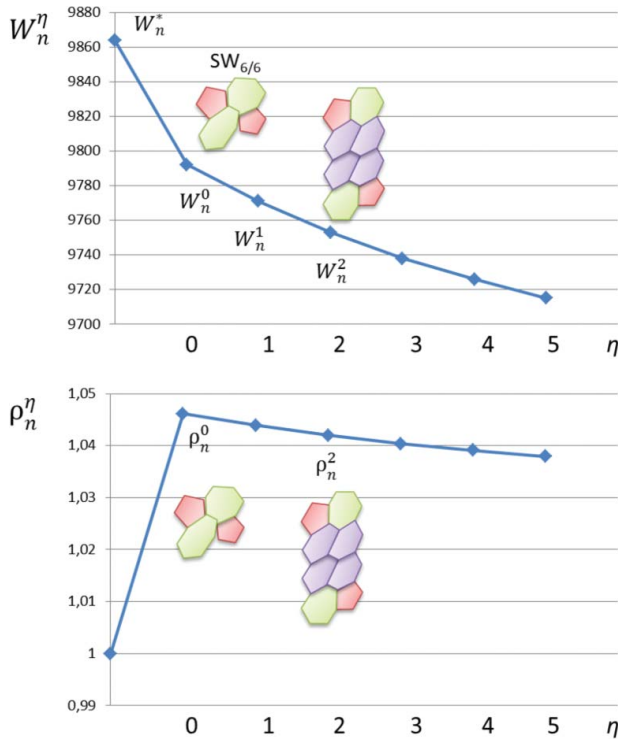

Figure 3. (a) Top. The topological potential W_n^η is computed for the SWw defect propagating in the hexagonal graph, in order to simulate the signal transmission in a neuron mesh equipped with $n = 72$ elements. $SW_{6/6}$ originates two 5|7 pairs at $\eta = 0$, then $SW_{6/7}$ splits them, by swapping one of the 5|7 two pairs with a pair of hexagons ($\eta = 1$). Further $SW_{6/7}$ rotation propagates the signal. Lattice configurations are depicted for $\eta = 0$ and $\eta = 2$; the initial value W_n^* corresponds to the pristine hexagonal mesh. (b) Bottom. Analogous variation of topological potential ρ_n^η for a SWw defect propagating in the periodic neuron mesh with $n = 72$ elements. The cost of the $SW_{6/6}$ rotation peaks at $\eta = 0$, whereas the $SW_{6/7}$ flips are followed by a gain favoring the propagation of the signal. The perfect symmetry of the pristine hexagonal mesh is testified by the value $\rho_n^* = 1$.

microcolumnar barcode predicted by a fullerene-like brain will be easily testable, once more powerful high density neurotechniques will be available, capable of capturing the simultaneous activity of large populations of microcolumnar pyramidal neurons (36). To make an example, if we were able to evaluate the microcolumnar pyramidal neurons that fire during every mental activity (e.g., visual tasks, emotions, and so on) we would achieve a fullerene-like structure filled with the corresponding activated nodes, therefore attaining a series of different grids or matrices (each one standing for a mental function).

Such powerful tools could be, in a near future, applied to the assessment of neural networks, in order to achieve a double task: improving our understanding of biological brain function in situ, and building more powerful artificial machines able to simulate cortical activities.

Conflict of interest

The authors declare that they have no conflict of interest.

References

1. Mountcastle, V. B. (1997) The columnar organization of the neocortex. *Brain*, 20 (4): 701–722.
2. Jones, E. G. (2000) Microcolumns in the cerebral cortex. *PNAS*, 97 (10): 5019–5021.
3. Casanova, M. F., El-Baz, A., and Switala, A. (2011) Laws of conservation as related to brain growth, aging, and evolution: symmetry of the minicolumn. *Front Neuroanat.* 26(5): 66.
4. Babic, D., Bassoli, S., Casartelli, M., Cataldo, F., Graovac, A., Ori, O., and York, B. (1995) Generalized Stone-Whales transformations. *Mol. Simul.*, 14: 395–401.
5. Ori, O., Putz, M. V., Gutman, I., and Schwerdtfeger, P. (2014) Generalized Stone-Wales transformations for fullerene graphs derived from berge's switching theorem. In *Ante Graovac — Life and Works*. Gutman, I., Pokric, B., Vukicevic, D. (eds.), 259–272.
6. Koorepazan-Moftakhar, F., Ashrafi, A. R., Ori, O., and Putz, M. V. (2015) *Geometry and Topology of Nanotubes and Nanotori. Exotic Properties of Carbon Nanomatter.* Vol. 8 of the series Carbon Materials: Chemistry and Physics. pp 131–152.
7. Turpin, A., Sampson, G.P., and McKendrick, A. M. (2009) Combining ganglion cell topology and data of patients with glaucoma to determine a structure–function map. *Invest Ophthalmol Vis Sci.* 50(7): 3249–3256.
8. Gomez-Ballesteros, J. L., Burgos, J. C., Lin, P. A., Sharma, R., Balbuena, P. B. (2015) Nanocatalyst shape and composition during nucleation of single-walled carbon nanotubes. *RSC Adv.* 5(129): 106377–106386.
9. Stam, C. J. and Reijneveld, J. C. (2007) Graph theoretical analysis of complex networks in the brain. *Nonlinear Biomed. Phys.*, 5; 1(1):3.
10. Köster, U., Sohl-Dickstein, J., Gray, C. M., and Olshausen, B. A. (2014) Modeling higher-order correlations within cortical microcolumns. *PLoSComputBiol*, 10(7): e1003684.
11. Singh, G., Memoli, F., Ishkhanov, T., Sapiro, G., Carlsson, G., and Ringach, D.L. (2008) Topological analysis of population activity in visual cortex. *J. Vision*, 8(8): 11–18.
12. Tozzi, A. and Peters, J. F. (2016) A topological approach unveils system invariances and broken symmetries in the brain. *J. Neurosci. Res.*, 94 (5): 351–65. doi:10.1002/jnr.23720.
13. Giusti, C., Ghrist, R., Bassett, D.S. (2016) Two's company, three (or more) is a simplex. Algebraic-topological tools for understanding higher-order structure in neural data. *J. Comput. Neurosci.* 41: 1–14.
14. Zhang, Z., Kutana, A., Yang, Y., Krainyukova, N.V., Penev, E.S., and Yakobson, B.I. (2016) Nanomechanics of carbon honeycomb cellular structures. *Carbon*, http://dx.doi.org/10.1016/j.carbon.2016.11.020.
15. Schwerdtfeger, P., Wirz, L., and Avery, J. (2015) The Topology of fullerenes. *Wiley Interdiscip. Rev.: Comput. Mol. Sci.*, 5: 96–145.
16. Chuang, C., Fan, Y-C., and Jin, B-J. (2009) Generalized classification scheme of toroidal and helical Carbon nanotubes. *J. Chem. Inf. Model.*, 2009, 49(2): 361–368. doi: 10.1021/ci800395r.
17. Fowler, P. W., Curl, R. F., and Murrell, J. N. (1993) Systematics of fullerenes and related clusters [and Discussion], philos. *Trans.: Phys. Sci. Eng.* 43(1667): 39–52.
18. Fowler, P. W., Rogers, K. M., Fajtlowicz, S., Hansen, P., and Caporossi, G. (2001) Facts and conjectures about fullerene graphs: Leapfrog, cylinder and Ramanujan fullerenes, In A. Benen et al. (Eds.), *Algebraic Combinatorics and Applications*, Springer.
19. Todeschini, R. and Consonni, V. (2000) *Handbook of Molecular Descriptors.* Wiley-VCH: Weinheim, Germany.
20. Ori, O., Cataldo, F., and Graovac, A. (2009) Topological ranking of C28 fullerenes reactivity. *Fullerenes, Nanotubes Carbon Nanostructures*, 17(3): 308–323. doi: 10.1080/15363830902782332.
21. Vukicevic, D., Cataldo, F., Ori, O., and Graovac, A. (2011) Topological efficiency of C66 fullerene. *Chem. Phys. Lett.*, 501(4–6): 442–445.
22. Graovac, A., Ashrafi, A. R., and Ori, O. (2014) Topological efficiency approach to fullerene stability—case study with C_{50}. *Advances in Mathematical Chemistry and Applications*, 2: 3–23. Subash C. Basak, Guillermo. Restrepo, and Jose L. Villaveces (Eds) Bentham Science Publishers.
23. Ori, O., Cataldo, F., and Putz, M. V. (2011) Topological anisotropy of stone-wales waves in graphenic fragments. *Int. J. Mol. Sci.* 12: 7934–7949; doi:10.3390/ijms12117934.
24. Matoušek, J. (2003) *Using the Borsuk-Ulam Theorem.* Springer-Verlag: Berlin, ISBN 978-3-540-00362-5.

25. Mitroi-Symeonidis, F-C. (2015) Convexity and sandwich theorems. *Eur. J. Res. Appl. Sci.*, 1: 9–11
26. Tozzi, A. (2016) Borsuk-Ulam Theorem Extended to Hyperbolic Spaces. In *Computational Proximity. Excursions in the Topology of Digital Images*, edited by J. F. Peters, 169–171. doi:10.1007/978-3-319-30262-1.
27. Tozzi, A., Fla, Tor, and Peters, J. F. (2016) Building a minimum frustration framework for brain functions in long timescales. *J. Neurosci. Res.* 94(8): 702–716.
28. Schwerdtfeger, P., Wirz, L., and Avery, J. (2013) Program FULLERENE a program for creating fullerene structures and for performing topological analyses. *J. Comput. Chem.*, 34: 1508–1526.
29. Opris, I. and Casanova, M. F. (2014) Prefrontal cortical minicolumn: From executive control to disrupted cognitive processing. *Brain.* 2014 Jul;137(Pt 7):1863–75. doi: 10.1093/brain/awt359.
30. Casanova, M. F., El-Baz, A., and Switala, A. (2011) Laws of conservation as related to brain growth, aging, and evolution: Symmetry of the minicolumn. *Front Neuroanat.* 26(5):66. doi: 10.3389/fnana.2011.00066.
31. Cruz, L., Urbanc, B., Inglis, A., Rosene, D. L., and Stanley, H. E. (2008) Generating a model of the three-dimensional spatial distribution of neurons using density maps. *Neuroimage.* 40(3): 1105–1115.
32. Peters, A. and Kara, D. A. (1987) Neuronal composition of area 17 of rat visual cortex. iv. the organization of pyramidal cells. *J. Comparative Neurology.* 260(4): 573–590.
33. Peters, A. and Sethares, C. (1991) Organization of pyramidal neurons in area-17 of monkey visual-cortex. *J. Comparative Neurology.* 1991;306(1): 1–23.
34. Gabbott, P. L. A. (2003) Radial organization of neurons and dendrites in human cortical areas 25, 32, and 32′. *Brain Res.* 992: 298–304.
35. Hashimoto, A., Suenaga, K., Gloter, A., Urita, K., Iijima, S. (2004) Direct evidence for atomic defects in graphene layers. *Nature*, 19;430 (7002): 870–3.
36. Köster, U., Sohl-Dickstein, J., Gray, C. M., and Olshausen, B. A. (2014) Modeling higher-order correlations within cortical microcolumns. *PLoSComputBiol.*, 10(7): e1003684.